energies

MDPI

Article

Gasification of *Psidium guajava* L. Waste Using Supercritical Water: Evaluation of Feed Ratio and Moderate Temperatures

Sandro González-Arias [1], Abel Zúñiga-Moreno [2], Ricardo García-Morales [1], Octavio Elizalde-Solis [1,*], Francisco J. Verónico-Sánchez [1] and Sergio O. Flores-Valle [1]

[1] Departamento de Ingeniería Química Petrolera and Sección de Estudios de Posgrado e Investigación, Escuela Superior de Ingeniería Química e Industrias Extractivas, Instituto Politécnico Nacional, UPALM, Edificio 8, Lindavista, Gustavo A. Madero, Ciudad de Mexico C.P. 07738, Mexico; mandro_891@hotmail.com (S.G.-A.); richo_garcia@hotmail.com (R.G.-M.); javi.ibq@hotmail.com (F.J.V.-S.); sergioodin@gmail.com (S.O.F.-V.)

[2] Laboratorio de Investigación en Fisicoquímica y Materiales, Departamento de Ingeniería Química Industrial, Escuela Superior de Ingeniería Química e Industrias Extractivas, Instituto Politécnico Nacional, UPALM, Edificio Z-5, 2° piso Lindavista, Gustavo A. Madero, Ciudad de Mexico C.P. 07738, Mexico; azunigam@ipn.mx

* Correspondence: oelizalde@ipn.mx or octavioel@yahoo.com.mx; Tel.: +52-55-5729-6000 (ext. 55120 or 55124)

Abstract: Biomass waste, as raw material for renewable energy, is an attractive alternative since it does not compete with human food supply. An emerging alternative for its treatment is supercritical water gasification (SCWG), due to the high moisture content of some types of biomass. On this regards, guava fruit (*Psidium guajava* L.) is one of the most wasted agro-food products in Mexico. This motivated us to evaluate gasification of guava waste on dry biomass base under supercritical water conditions for the first time, with the aim of analyzing the impact of moderate temperatures and feed ratios as reaction parameters on gas products. Temperature was varied in the range of 673.15–773.15 K and using a batch reactor loaded with biomass:water (B:W) mass ratios of 1:1, 1:4, and 1:6. Furthermore, the obtained solid, liquid, and gas phase products were characterized. Hydrogen (H_2), carbon dioxide (CO_2), carbon monoxide (CO), methane (CH_4), ethane (C_2H_6), propane (C_3H_8), and butane (C_4H_{10}) were identified in gas phase and quantified by means of a gas chromatograph equipped with a TCD detector. Liquid and solid phase products were subjected to Fourier Transform Infrared spectroscopy analyses. This preliminary research indicated that high temperature operation and high biomass:water mass ratio enhanced gas yields (mol/kg) of about 4.137 for CH_4, 6.705 for CO_2, and 7.743 for H_2; whereas the selectivity and gas efficiency for hydrogen was 65.26% and 58.94%, respectively.

Keywords: supercritical; gasification; water; biomass waste; *Psidium guajava* L.

Citation: González-Arias, S.; Zúñiga-Moreno, A.; García-Morales, R.; Elizalde-Solis, O.; Verónico-Sánchez, F.J.; Flores-Valle, S.O. Gasification of *Psidium guajava* L. Waste Using Supercritical Water: Evaluation of Feed Ratio and Moderate Temperatures. *Energies* **2021**, *14*, 2555. https://doi.org/10.3390/en14092555

Academic Editor: Dmitri A. Bulushev

Received: 12 April 2021
Accepted: 27 April 2021
Published: 29 April 2021

1. Introduction

Gasification via supercritical water is an alternative technology in gasification of biomass with high moisture content. Some remarkable aspects for reactions in SCWG are the lower operating temperature in comparison with the corresponding for conventional gasification or pyrolysis, the suitable solvating power for water focused on organic reactants, the inhibition of reactions as polymerization, and the high hydrogen-production in detriment of carbon monoxide content at high temperatures.

A great variety of biomass has water content higher than 80%. SCWG processes exhibit some advantages due to the supercritical water properties (critical temperature, 647.10 K; critical pressure, 22.06 MPa), such as high diffusion rates, low viscosity, and low dielectric constant. These characteristics make water an excellent solvent for organic materials, and takes part on the hydrogen bonds weakening to contribute hydrogen production [1]. Nowadays, organic/inorganic residues have been highlighted because its exploitation

can generate value-added products instead of waste disposal. In this concern, waste biomass can be used as wet feedstock for fuel gas generation. The exploitation of renewable resources to produce less-pollutant fuels are a solution to avoid complete dependence on fossil fuels since combustion of petroleum fractions provokes environmental pollution by greenhouse gases.

Regarding the Mexican agricultural sector, a serious problem on post-harvest crop products is the huge losses on fruits during the food production chain stages (from farmers to final customers). Based on official reports from the Secretary of Social Development (Secretaría de Desarrollo Social, Mexico) in 2015, the total food waste was 10,000,431 tons per year equivalent to 37.26% of total production. Guava fruit (*Psidium guajava* L.) was the most wasted fruit in Mexico, about 57.70% of its national production [2], which creates an opportunity area for this waste. It can be treated via diverse chemical processes to generate high value-added products.

Taking advantage of water content, biomass waste can be utilized in a gasification process using supercritical water to obtain gaseous fuels or syngas, (which contains hydrogen) depending on the operation conditions. Water would act as solvent and reactant at supercritical conditions; hence, biomass might not require rigorous pretreatment. The first approaches have studied SCWG with model compounds (lignin, fructose, cellulose, hemicellulose, and glucose). Furthermore, vast efforts have been carried out using organic or inorganic "real" biomass, such as plastic material, petroleum fractions, municipal or industrial wastewater, and sludge, as well as some organic residues from agricultural, animal, and food sectors. About experiments, fuel synthesis has been performed above critical temperature of water up to 1123 K in catalytic/non-catalytic batch or continuous flow reactors made of different materials. All these parameters are aimed to describe the reaction mechanism, look for the optimum operating conditions, and perform numerical simulation [3–15].

Composition and content of products via SCWG depend on the reaction conditions and biomass composition. For instance, lignocellulosic biomass is typically constituted by cellulose (45–50%), hemicellulose (20–25%) and lignin (20–25%). The reaction mechanism that induces water is complex at these conditions, as demonstrated elsewhere [3–15]. Initially, biomass material conversion produces intermediates by hydrolysis and the water solvating power effect. Consequently, these compounds are fragmented and cracked to produce gaseous components and small molecules [16]. The overall reaction can be summarized according to Equation (1), focused on hydrogen [17,18]:

$$CH_xO_y + (2 - y)\, H_2O \rightarrow CO_2 + (2 - y + x/2)\, H_2 \quad (1)$$

Specific reactions for gas production are steam reforming, hydrolysis, reforming, water-gas shift, thermal decomposition, hydro-pyrolysis, oxidation, hydrogenation, methanation, and polymerization. The improvement or decreasing of these reactions is clearly dependent on temperature, biomass:water concentration, and biomass nature. The most important are:

Steam reforming

$$CH_xO_y + (1 - y)\, H_2O \rightarrow CO + (1 - y + x/2)\, H_2 \quad (2)$$

Water-Gas shift

$$CO + H_2O \rightarrow CO_2 + H_2 \quad (3)$$

CO Methanation

$$CO + 3\, H_2 \rightarrow CH_4 + H_2O \quad (4)$$

CO_2 Methanation

$$CO_2 + 4\, H_2 \rightarrow CH_4 + 2\, H_2O \quad (5)$$

CO Hydrogenation

$$CO + 2\, H_2 \rightarrow CH_4 + 0.5\, O_2 \quad (6)$$

Boudouard

$$2\,CO \rightarrow C + CO_2 \quad (7)$$

$$CO_2 \rightarrow C + O_2 \quad (8)$$

Lignocellulosic compounds take part on the intermediate reactions; lignin hydrolysis on Equation (5) also produces phenolic compounds, which are subsequently converted to gas compounds by steam reforming.

Cellulose hydrolysis

$$(C_6H_{10}O_5)_n + n\,H_2O \rightarrow n\,C_6H_{12}O_6 \quad (9)$$

Glucose reforming

$$C_6H_{12}O_6 \rightarrow 6\,CO + 6\,H_2 \quad (10)$$

Lignin hydrolysis

$$(C_{10}H_{10}O_3)_n + n\,H_2O \rightarrow n\,C_{10}H_{12}O_4 \quad (11)$$

Concerning reutilization of real waste biomass. Some agro-food residues that have been studied elsewhere on dry or wet basis under supercritical water gasification are fruit pulp, peach scrap, aloe vera rind, coconut shell, sugarcane bagasse, malt spent grains, bio-oil, food waste, and peel from banana, lemon, orange, or pineapple. In certain applications, those biomasses were gasified under activated carbon, Ru/C, K_2CO_3, NaOH, $KHCO_3$, Na_2CO_3, KOH, $FeCl_3$ and nickel-base materials as catalysts, even dosing additives in food waste feedstocks [19–30]. For the best of our knowledge, Silveira-Junior et al. have recently carried out fast pyrolysis from seed guava in the range of 623.15–873.15 K focused on levoglucosan. Biochar production raised at low temperature, the opposite occurred with liquid–phase generation whose maximum was attained at high temperature, whereas carbon dioxide was in the interval of 2.51–5.15% [31]. Therefore, our interest is centered in valorization of guava fruit waste under SCWG. The goal of our current study was to evaluate the effect of moderated temperatures (673.15–773.15 K) and biomass concentration (1:1, 1:4, 1:6) on the value-added chemicals yielded in gas, liquid and solid phases. As first approach, guava fruit waste was used in dry base biomass.

2. Materials and Methods

Overripe pink guava fruit (*Psidium guajava* L.) was collected from the state of Morelos, Mexico. The moisture content was achieved by a 915 KF Ti-Touch (Metrohm, Switzerland). The fruits were dehydrated in an oven and grinded up with the aim of avoiding an heterogenous sample lot. Biomass dry particles were estimated to have a geometric mean diameter of 0.624 mm. The water was distilled-grade and sulfuric acid was analytical grade (95–98%). Chemicals used as standards for calibration of analytical instrument were of high purity.

The particle size distribution of guava fruit was evaluated based on ASABE standard method S319.4 [32] of determining and expressing fineness of feed materials by sieving. Afterwards, biomass was characterized by ash content as per ASTM E-1755-95 standard test method, insoluble dietary fiber based on the method proposed by Claye et al. [33], high heating value (HHV) performed in a 6200 bomb calorimeter (Parr, USA), elemental C, O, H, N, S analysis carried out with a FLASH 2000 (Thermo Scientific, USA), total organic carbon (TOC) content by using a TOC-L (Shimadzu, Japan), and a Frontier FT-IR spectroscopy (PerkinElmer, USA) using 2 cm^{-1} of resolution. Thermogravimetric analysis (TGA) and differential calorimetry scanning (DSC) were performed on a STA PT 1000 (Linseis, Germany) at a heating rate of 11 K/min in a temperature range from 298.15 to 853.15 K and under argon atmosphere. The TGA allowed estimating the devolatilization behavior of the guava fruit waste by calculating the differential weight loss.

Supercritical water gasification reactions were conducted in a batch reactor made of Inconel 625 alloy. A schematic diagram is illustrated in Figure 1. The equipment is mainly

constituted by a reactor vessel of 150 cm^3 {1} internal volume, a stirring motor {2} with a stirring shaft and a three-blade impeller, needle valves (Vi), an electric heating resistance {3}, a manometer {4}, two K-type thermocouples {5,6}, a PID temperature controller {7}, a computer {8}, internal cooling service {9} coupled to a circulating liquid bath, a relief valve {10}, a stainless steel filter of 0.5 cm {11}, a steam trap {12}, an autoclave of 30 cm^3 volume {13}, an analytical balance {14} and a separator {15}.

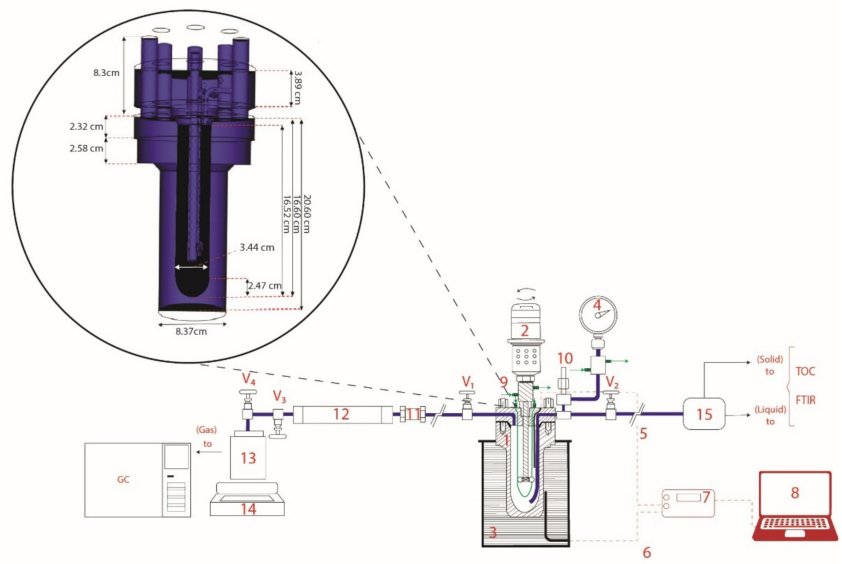

Figure 1. Schematic diagram of the reactor.

Supercritical water gasification of guava fruit waste consisted on feeding into the reactor 100 g of mixture constituted by water and biomass on dry base, different biomass:water mass ratio were evaluated (B:W = 1:1, 1:4, 1:6), in order to reach high pressure conditions reported in the interval of 25.0–45.0 MPa. Weightings were measured in an analytical balance. Then, the reactor was hermetically sealed, and air was evacuated throughout a vacuum pump. Afterwards, the reactor was heated by an electrical furnace at a rate of 4 K/min to reach the desired temperature in the range of 673.15–773.15 K. Reaction conditions were kept for 60 min until the desired temperature was attained. Operating pressure depended on the temperature and the total volume of the biomass:water. Finally, the reaction was stopped by removing the reactor from the electrical heating resistance and a sudden cooling down to room temperature. Experiments were duplicated in order to check reliable conditions and results are reported as the average of repetitive runs.

Products were obtained in gas, liquid, and solid phases and were quantified gravimetrically in an analytical balance. The upper needle valve was opened to allow the gas flows throughout the stainless-steel filter and subsequently the molecular sieve 5A trap, to suppress the presence of solids and moisture. Then, the dried gas was collected in a high-pressure cell for weighing purposes.

The reactor was opened by removing the cover to gather liquid and solid residues. Preliminary experiments demonstrated the formation of four-phases: gas, aqueous, organic liquid, and solid; Nevertheless, the formation of two liquid phases was avoided in the reported results by adding two drops of sulfuric acid in liquid–phase. Hence, the ionization of organic acids and the formation of additional insoluble materials was inhibited. The liquid and solid were separated, the first one was filtered, and the second one was subject to evaporation.

The composition of gas effluent was analyzed in a gas chromatograph GC-7890B (Agilent, USA) equipped with a TCD detector and two columns; RT-XL packed and molsieve 13x capillary columns connected in series with argon as carrier gas. Temperatures for the TCD and injector were 523.15 K. The temperature gradient for the oven was set initially to 313.15 K for 4 min, and then a rate of 15 K/min was applied to reach 513.15 K

for 11 min, followed by another ramp of 30 K/min set to reach 393.15 K during 2.6 min. Finally, gas compounds were quantified by external calibration of the TCD, evaluating the retention times using pure compounds as standards. Liquid products were characterized qualitatively and quantitatively by FT-IR spectroscopy and total organic carbon (TOC), in that order. Meanwhile solid phase was analyzed by FT-IR.

3. Results

3.1. Biomass Characterization

Guava sample was subject to moisture content on wet basis. The remaining characterization results on dry basis such as geometric mean diameter (gmd), ash content, high heating value, TOC content, as well as ultimate and structural analyses are also listed in Table 1. The lignocellulosic biomass had a great content in C and O, low content in hydrogen, and slight amount of nitrogen and sulfur. The structure was predominantly constituted by hemicellulose and lignin with low content of cellulose. Some of these parameters are reported elsewhere by different research groups [34,35].

Table 1. Guava fruit waste characterization.

Ultimate Analysis/wt%					**Moisture [1]/wt%**	**gmd/mm**
C	H	N	S	O [2]		
42.19	6.19	0.89	0.02	50.71	82	0.624
Structural Analysis/wt%				**Ash/wt%**	**HHV/kJ·kg^{-1}**	**TOC/wt%**
Cellulose	Hemicellulose	Lignin	Extracts			
2.70	64.60	26.10	3.68	2.92	17250.6	33.5

[1] Wet basis. [2] O = 100–C–H–N–S–ash.

The thermal exposure of guava under atmospheric pressure was studied by thermogravimetric analysis and differential scanning calorimetry. Sample weight loss was recorded as increasing temperature to obtain thermograms and differential thermogravimetric curves at controlled heating rate as depicted in Figure 2. The combustion process profile depended on the composition and nature of sample. The organic matter was broken down into stages: drying, as well as active and passive pyrolysis. The organic biomass devolatilization profile were separated into several temperature-dependent zones.

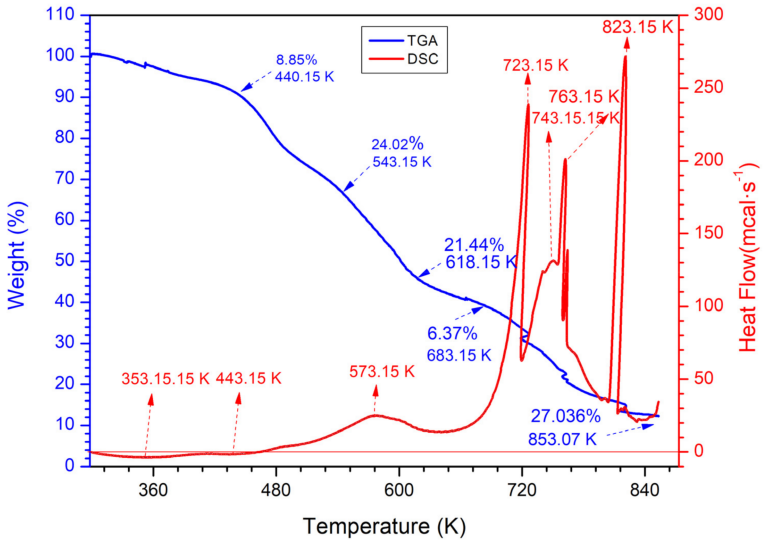

Figure 2. Thermal analysis of guava fruit (*Psidium guajava* L.) waste.

The first zone for the TGA curve had a weight loss of 8.85% up to around 440.15 K, caused by the release of moisture and volatile compounds. Afterwards, the second zone

covered a slope in the interval from 440.15 K to 618.15 K, which represented a weight loss of 45.46%. It was associated with the devolatilization of components hemicellulose and cellulose degradation took place as well as lignin combustion. Hemicellulose was easier to be degraded than the others at these temperatures since it is mainly constituted by saccharides with amorphous structures, rich in branches. The last zone showed different slopes that began at 618.15 up to 853.15 K whose weight loss was about 33.41%. Lignin decomposition ended and was the main biomolecule that promoted biochar formation. The greater thermal stability on lignin structure was demonstrated compared with cellulose and hemicellulose. Besides, aromatic compounds predominated since the C–C bonds in phenylpropane [36,37].

The behavior of the differential scanning calorimetry analysis exhibited two endothermic broad peaks related to the energy required for evaporating moisture at 353.15 K and volatile compounds at 443.15 K. Energy release occurred at 573.15 K, which confirmed the degradation of hemicellulose and cellulose, as well as lignin, but partially [37–39]. Afterwards, four additional devolatilization sharp peaks were observed at 723.15, 743.15, 763.15, and 823.15 K; these could still be produced by the thermal decomposition of the remaining lignin [39,40]. Besides, the rupture of biomolecules (depolymerization reactions) such as xylan [41,42], biochar formation [43] and gas release [39,42,44], the combustion of complex branched (including aromatic rings), thermal stable structures [39,44], and ash [39–45] could contribute within this intense exothermic energy. Temperatures higher than 853.15 K were not tested since no significant peaks have not been reported previously based on the analysis carried out by Athmaselvi et al. [46].

Guava samples were also analyzed by Fourier Transform Infrared spectroscopy, a representative spectrum is illustrated in Figure 3 where the adsorption bands were associated with the functional groups of complex compounds. Emphasis was made on the polysaccharides listed in Table 2 as cellulose, hemicellulose, and lignin, but the samples also contained other components identified elsewhere like pectin, proteins, and flavonoids [47–50].

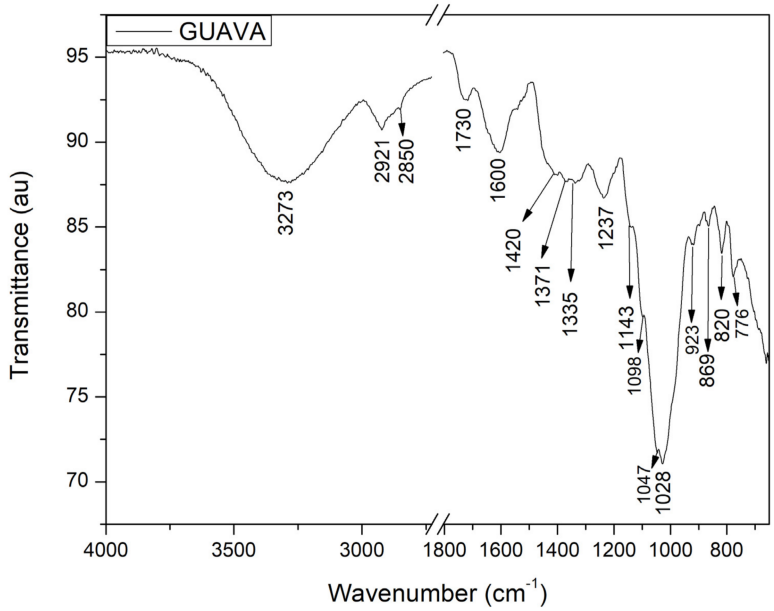

Figure 3. FT-IR spectrum for guava fruit waste.

Table 2. Absorption frequencies of functional groups in the guava fruit waste.

Wavenumber/cm^{-1}	Functional Group	Polymer	Reference
3273	OH, NH	Carbohydrates, lignin, hemicellulose, cellulose	[50–54]
2921	CH_2 aliphatic	Carbohydrates, lignin	[47,52,53]
2850	CH_2 aliphatic	Pectin, protein	[47,52]
1730	C=O ester group	Hemicellulose	[47,50,55,56]
1600	C=O, aromatic	Lignin	[55–58]
1420	Aromatic, C–H	Cellulose, hemicellulose, lignin	[56,57,59–61]
1371	C–H	Cellulose, hemicellulose	[56,59–62]
1335	CH–, OH	Cellulose, hemicellulose, lignin	[55,56,63]
1237	C–O, C–O–C	Carbohydrates	[53,64,65]
1143	Aromatic C–H, OH, C=O	Lignin	[56,65]
1098	C–O–H, C–O	Cellulose, hemicellulose, lignin	[58,66]
1047		Cellulose, hemicellulose	[56,62,65,67]
1028	C_3–O_3H, C–O	Cellulose, hemicellulose, lignin	[50,52,55,65]
923	C_6–O_6H, C–O, C=C, C–C–O	Lignin	[56,68]
869	Aromatic, C–H	Hemicellulose	[56,65,66]
820	C_2–H	Lignin	[56,65,66]
776	C–H	Carbohydrates and lignin	[53,69]

The strong broad peak at 3273 cm^{-1} denoted the phenolic and aliphatic hydroxyl group stretching vibration; NH stretching of the amine group indicated the amino acid components [50–54]. The CH_2 asymmetrical and symmetrical stretching for alkane groups were associated with the medium peak at 2921 cm^{-1} and the weakness signal at 2850 cm^{-1}, respectively [47,52,53]. The weak peak around 1730 cm^{-1} corresponded to the carbonyl C=O stretching vibration of different groups such as acetyl, aldehydes, ketones and carboxylic acids [47,50,55,56]. The stretch of the carbonyl (C=O) conjugated with the aromatic skeleton of phenylpropane appeared for the medium signal at 1600 cm^{-1} of wavelength [55–58]. The weak signal at 1420 cm^{-1} indicated CH_3 bending vibrations, CH_2 symmetrical deformations and C–H in plane deformation with aromatic structure vibration [56,57,59–61]. The relative weakness that lied at 1371 cm^{-1} was ascribed to C–H bending of alkanes [56,59–62]. The signal at 1335 cm^{-1} was associated with OH in-plane bending and CH_2 wagging of alcohols and alkanes [55,56,63]. The sharp signal noticed at 1237 cm^{-1} corresponded to C–O, C–O–C bonds indicating the presence of carboxylic acids and ethers [53,64,65]. The weak peak observed at 1143 cm^{-1} presented aromatic C–H in plane bending, OH and C=O stretches [56,65]. The weak shoulder absorption band observed at 1098 cm^{-1} could be attributed to the C–O–H bending modes and C–O, suggesting the presence of alcohol groups [58,66]. The peak observed in 1047 cm^{-1} might be assigned to C_3–O_3H, and C–O stretching in C–O–C (ether) bonds [56,62,65,67]. The strongest sharp signal located around 1028 cm^{-1} was designated to C_6–O_6H, C–O, C=O, and C–C–O stretches denoting phenol, alcohol, and ester [50,52,55,65]. The 923 cm^{-1} weak signal indicated C–H out of plane for alkane group and aromatic [56,68]. The weak band sharpened at 869 cm^{-1} corresponded to deformation of the equatorial C_2–H bond of mannosyl residue, and the narrow peak at 820 cm^{-1} presented C–H out plane bending [56,65,66]. The peak at 776 cm^{-1} could be assigned to deformation C–H in aromatic of carbohydrates and lignin [53,69].

3.2. Supercritical Water Gasification

Products obtained in gas, liquid, and solid phases from gasification under supercritical water were obtained from the complex mechanism where simultaneous or in-series phenomena and reactions are taking place. The main reactions: hydrolysis, decomposition, reforming, water–gas shift, methanation, hydrogenation, and polymerization were summarized in Equations (1)–(11) and explained by Okolie et al. [17] and Safari et al. [18]. The upgrade or inhibition of a particular reaction varied according to the experimental conditions.

Products in gas phase from supercritical water gasification of waste guava fruit biomass evaluated at different conditions of mass ratio, temperature, and pressure are listed in Table 3 and depicted in Figure 4. The identified components, hydrogen, carbon dioxide, carbon monoxide, methane, ethane, propane, and butane, were analyzed by gas chromatography in terms of mole fraction (y_i) based on Equation (12), where n_i is the mole amount (n) for each chemical species (i). Nitrogen and oxygen were not detected.

$$y_i\ (\%) = n_i/(\sum_i n_i) \times 100 \quad (12)$$

Table 3. Conditions for gasification reactions and gas product composition using supercritical water.

Run	B:W [1]	*T*/K	*P*/MPa	y_{CH4}	y_{CO2}	y_{C2H6}	y_{C3H8}	y_{C4H10}	y_{H2}	y_{CO}
R1	1:1	673.15	27.8	9.0	72.6	1.4	0.3	0.2	13.4	3.0
R2	1:4	673.15	25.0	21.5	49.7	5.4	1.8	0.4	20.5	0.7
R3	1:6	673.15	25.5	26.3	45.0	2.1	0.3	–	20.2	6.1
R4	1:1	713.15	43.0	20.8	51.8	3.1	0.8	0.2	20.1	3.2
R5	1:4	713.15	45.0	19.9	50.5	2.7	0.7	0.2	23.7	2.5
R6	1:6	713.15	38.5	20.7	48.3	3.2	0.9	0.3	25.2	1.4
R7	1:1	773.15	44.5	12.3	58.1	3.0	0.9	0.4	21.2	4.0
R8	1:4	773.15	40.0	26.7	38.4	3.8	0.8	0.1	28.3	1.9
R9	1:6	773.15	42.0	21.1	34.2	2.6	0.6	0.1	39.5	1.9

[1] B:W denotes biomass:water mass ratio.

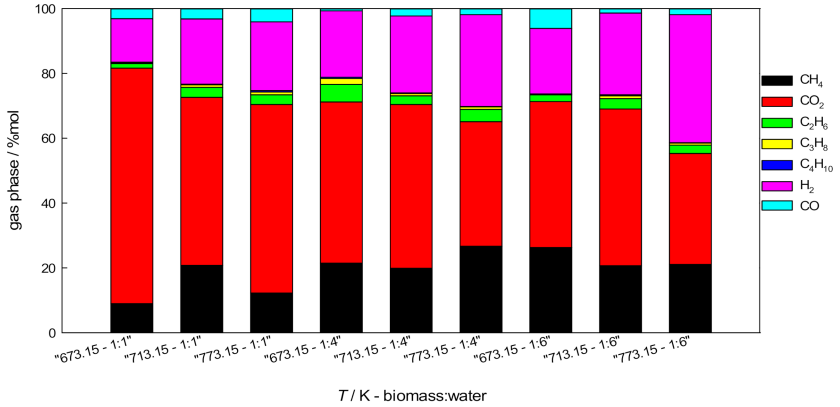

Figure 4. Gas phase products of SCWG from guava fruit waste biomass.

Besides, gas yields were calculated according to Equation (13); their values are presented in Table 4.

$$\text{gas yield (mol/kg)} = n_i/m_{\text{feed}} \quad (13)$$

where m_{feed} was referred to the mass of feed.

Table 4. Evaluation of gas yield.

Run	Gas Yield (mol·kg^{-1})						
	CH_4	CO_2	C_2H_6	C_3H_8	C_4H_{10}	H_2	CO
R1	0.211	1.696	0.033	0.008	0.005	0.313	0.070
R2	0.960	2.218	0.241	0.081	0.017	0.915	0.030
R3	1.979	3.384	0.161	0.019	–	1.520	0.457
R4	0.532	1.321	0.080	0.021	0.005	0.514	0.081
R5	1.361	3.458	0.182	0.046	0.011	1.623	0.168
R6	2.584	6.034	0.395	0.118	0.036	3.151	0.175
R7	0.520	2.465	0.128	0.039	0.018	0.900	0.171
R8	2.609	3.755	0.372	0.075	0.010	2.766	0.187
R9	4.137	6.705	0.501	0.119	0.025	7.743	0.376

In general, the lowest quantity was obtained for butane, and it was negligible in run R3. Carbon dioxide was the major component in all reactions, its highest content was reported at the lowest temperature and mass ratio; the mole fraction tended to decrease as mass ratio increased at fixed temperature and the opposite was observed at high temperatures at fixed mass ratio. Therefore, decarboxylation of acids and thermal decomposition were the dominant reactions among the others since a high rate of gasification of carbon and oxygen instead of hydrogen. Mole fraction for carbon monoxide was lower than 6.1%, it occurred at 673.15 K with 1:6 B:W mass ratio. The magnitude order for hydrocarbons was $CH_4 > C_2H_6 > C_3H_8 > C_4H_{10}$. Methane production was induced as temperature increases at 1:1 mass ratio; nevertheless, this behavior was not so remarkable at higher mass ratios because of three insights: the hydrogen production had been promoted, methanation was inhibited and nickel from reactor wall acted as catalyst during methane reforming. Significant changes were not identified for the other alkane quantities since steam reforming reaction and decompositions were taking place, but these were not so remarkable. Low hydrogen content was obtained at low mass ratio and the highest hydrogen production was obtained at 1:6 B:W mass ratio since high temperature and water content promoted the water-gas shift reaction in detriment of carbon dioxide formation. Temperature represented the greatest effect for obtaining gas since high temperature decreased solvent density drastically at supercritical conditions. Similar effect was caused in the ionic product promoting radical reactions such as hydrogenation, dealkylation, ring opening, polymerization by oligomer dehydrogenation. These reactions favored the structural compounds breakdown of biomass. In addition, high temperature upgraded energy needed to break carbon bonds and, hence, promoting the formation of light compounds such as methane and hydrogen.

Regarding carbon dioxide yield, the highest one was achieved at 773.15 K and 1:6 B:W mass ratio, but it diminished at lower temperature and mass ratio. Concerning H_2 and hydrocarbons, high temperature promoted raising on yields, but this parameter for ethane and heavier molecular weight hydrocarbons was so slight, besides low and variable yields for carbon monoxide were accomplished. The global yield was enhanced with temperature raising, so it would be suitable to explore higher temperature reactions.

The following parameters were calculated from gas quantification: hydrogen selectivity, hydrogen gasification efficiency (HGE), carbon gasification efficiency (CGE), and low heat value (LHV). Equations are detailed as follows:

H_2 selectivity (%) =

$$n_{H2}/(n_{CH4} + n_{CO2} + n_{CO} + n_{C2H6} + n_{C3H8} + n_{C4H10}) \times 100 \quad (14)$$

HGE (%) =

$$(4\, n_{CH4} + 2\, n_{H2} + 6\, n_{C2H6} + 8\, n_{C3H8} + 10\, n_{C4H10})/n_{H,feed} \times 100 \quad (15)$$

CGE (%) =

$$(n_{CH4} + n_{CO2} + n_{CO} + 2\, n_{C2H6} + 3\, n_{C3H8} + 4\, n_{C4H10})/n_{C,feed} \times 100 \quad (16)$$

LVH_{gas} ($kJ \cdot Nm^{-3}$) =

$$4.2\,(30\, n_{CO} + 25.7\, n_{H2} + 85.4\, n_{CH4} + 151.3\, n_{C2H6}) \quad (17)$$

The hydrogen selectivity calculated with Equation (14) is shown in Figure 5. Chemicals were subject to hydrolysis, reforming, and thermal decomposition. Monomers obtained from hydrolysis were subsequently involved in decomposition reactions to obtain low molecular weight chemicals, then these were decarboxylated to finally produce hydrogen and carbon dioxide The lowest selectivity was accomplished at low temperature and low mass ratio and it increased as mass ratio and temperature increased. The highest selectivity was reported at 773.15 K and 1:6 B:W mass ratio. This enhancement could be explained from an increase on bond cleavage, the bond gas products reactions, and the high water

concentration. A better promoting effect on steam reforming and water-gas shift reactions could be occurring in comparison with CO or CO_2 methanation reactions.

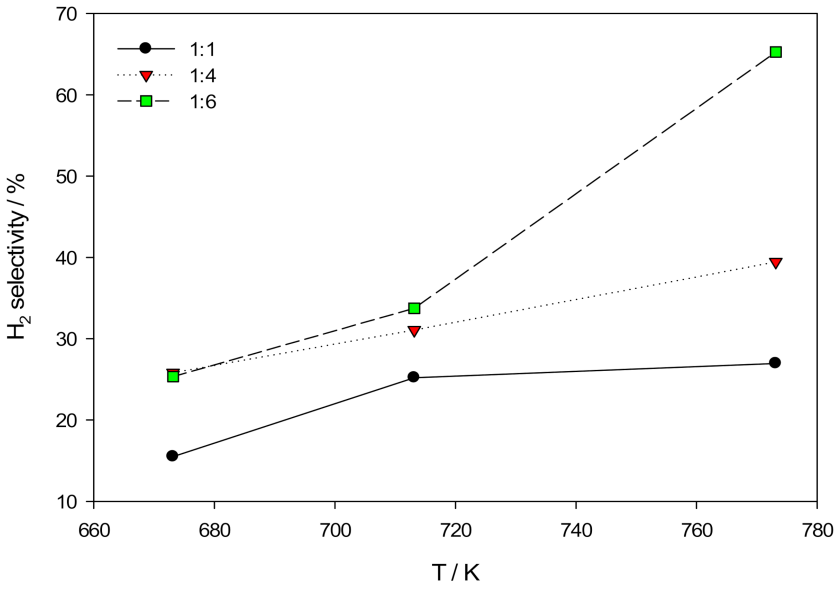

Figure 5. Hydrogen selectivity of SCWG from guava fruit waste at different B:W mass ratio.

Hydrogen gas efficiency and carbon gas efficiency are depicted in Figure 6, both were calculated using Equation (15), Equation (16), respectively. HGE and CGE were promoted by temperature and mass ratio increments. The highest values for hydrogen were obtained at 773.15 K and 1:6 B:W mass ratio. Gas efficiency for hydrogen were higher than those for carbon at the same conditions except for the lowest B:W mass ratio, 1:1. Nevertheless, the studied conditions did not accelerate the biomass hydrolysis and further conversion of the more complex components. The temperature conditions did not allow the decomposition of refractory chemicals and hence higher yields and efficiencies.

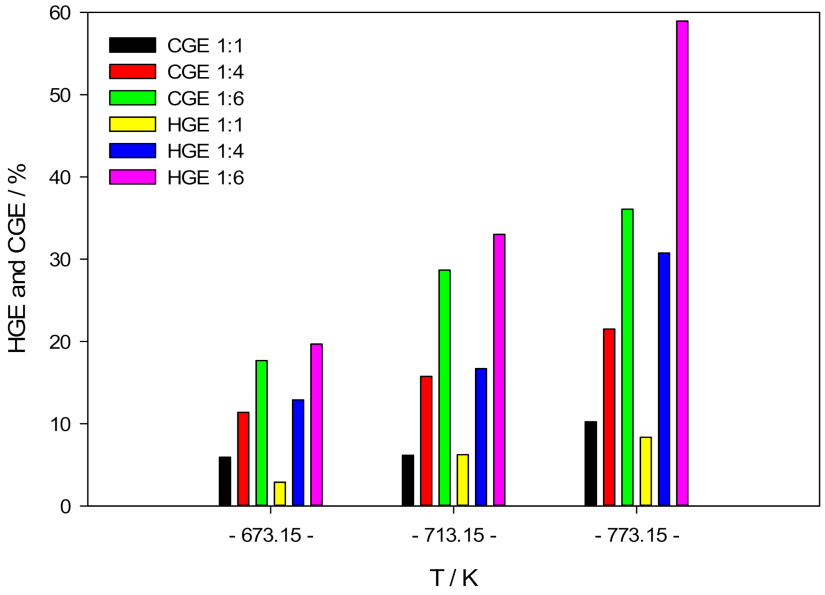

Figure 6. CGE and HGE of SCWG from guava fruit waste based on B:W mass ratio.

Finally, the LHV calculated based on Equation (17) is plotted in Figure 7 as a function of temperature and mass ratio. The lower LHV sets were observed for 1:1 in comparison with the other mass ratios. The low heat value tended to enhance in function of the mass ratio and temperature raising. Besides, the highest LHV was attained at highest temperature and mass ratio due to the high concentration and yield presented by H_2 at these conditions.

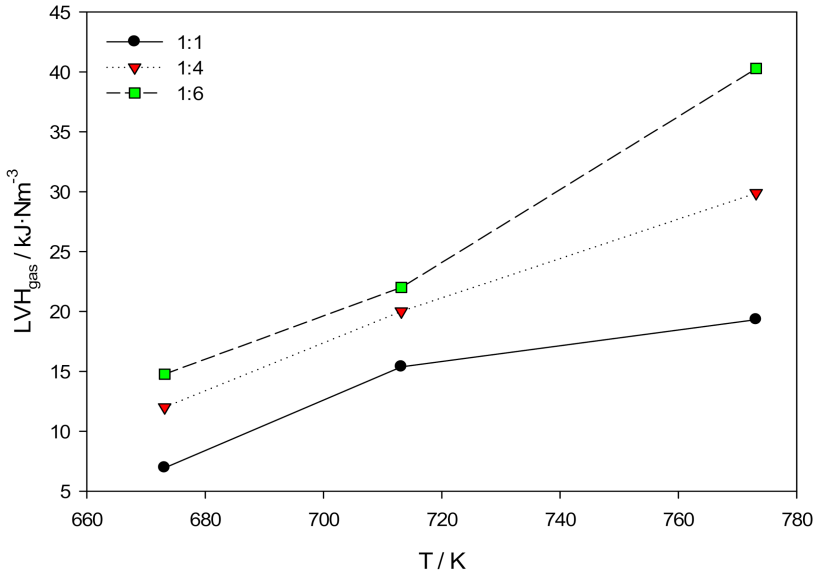

Figure 7. LHV of SCWG from guava fruit waste at different B:W mass ratios.

3.3. Liquid and Solid Products

Gasification also produced intermediates derived from incomplete conversion due to moderate temperatures. Some of them could be classified as ketones, aldehydes, alkanols, phenols, and carboxylic acids. The liquid-phase was initially obtained in different colors due to suspended solids; a yellowish mixture was gathered for all liquid samples after solid filtration. TOC analyses for the liquid-phase are shown in Figure 8.

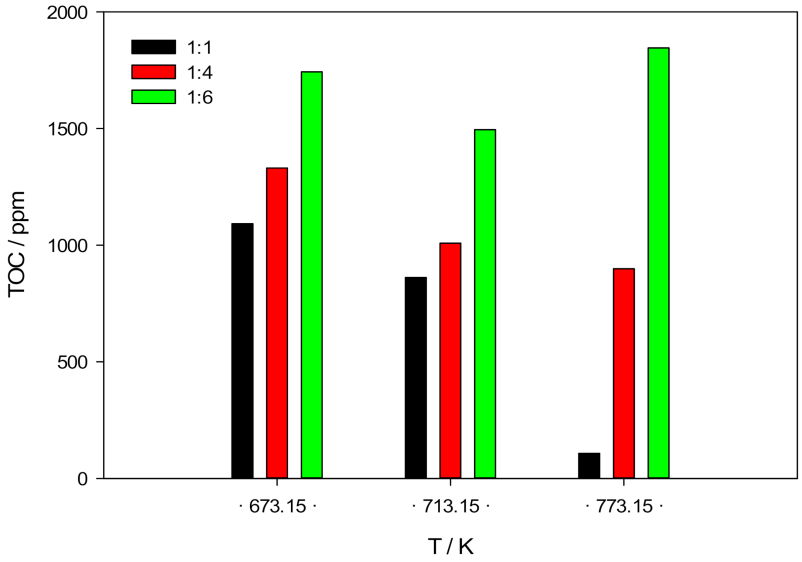

Figure 8. TOC analyses of liquid–phase products based on B:W mass ratio.

The TOC concentration was decreasing as temperature increased. Regarding the mass ratio, TOC concentration increased as water concentration was high. FT-IR spectra for liquid-phase products are illustrated in Figure 9.

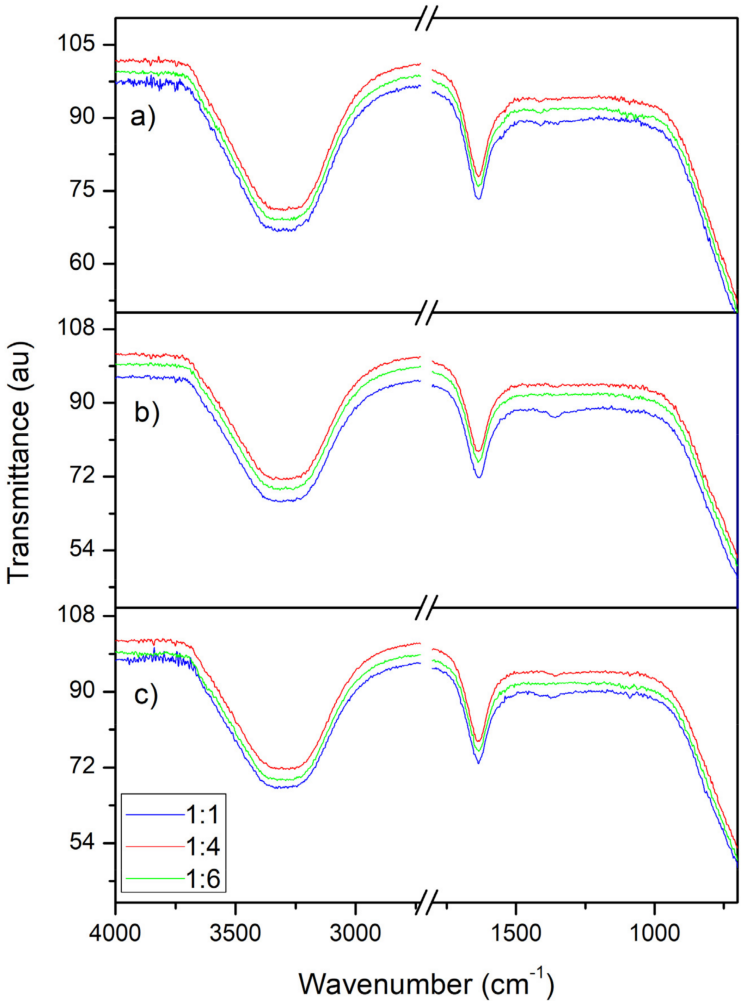

Figure 9. FT-IR spectra for liquid–phase products: (**a**) 673.15 K; (**b**) 713.15 K; (**c**) 773.15 K.

Two intense peaks were observed in the range of 3000–3600 cm^{-1} and at 1621 cm^{-1}. The first peak was associated to alcohol and carboxylic acid groups, and the second exhibited carboxylic acids, amides and heterocyclic compounds. Those analyses confirmed the presence of phenolic compounds and polycyclic aromatic hydrocarbons since refractory compounds could not be degraded at these the temperature conditions. Phenolic compounds were the most difficult chemicals to be decomposed and hence inhibited gas formation under supercritical water conditions. Besides, the high concentration of biomass on feed for 1:1 B:W mass ratio was not beneficial for a better gas yield during steam reforming or water-gas shift reactions since these reactions needed sufficient water as reactant.

FT-IR spectra for solid phase products are depicted in Figure 10 based on temperature and mass ratio.

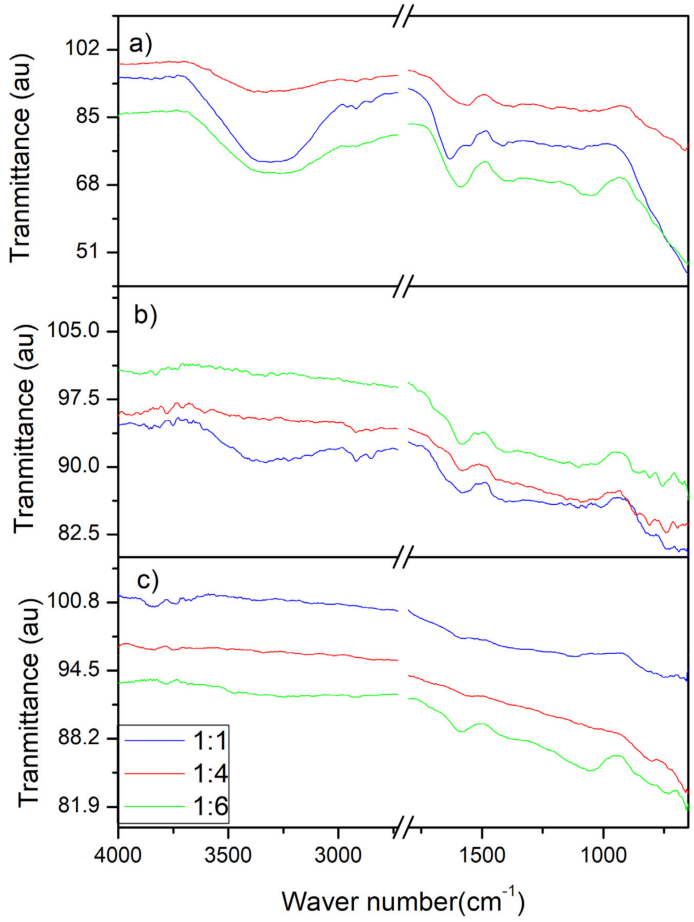

Figure 10. FT-IR spectra for solid phase products: (**a**) 673.15 K; (**b**) 713.15 K; (**c**) 773.15 K.

The temperature effect on the intensity of functional groups from biomolecules was remarkable in most of the peaks, and in others, these disappeared. For instance, the intensity of the highest peak between 3340 and 3600 cm^{-1} at 673.15 K represented alcohols and carboxylic acid groups. This peak was diminishing as temperature increased and it demonstrated the low gasification efficiency at 673.15 K, which was improved as temperature increased. The peak was suppressed at 773.15 K because of the dehydration effect. The same occurred for the peaks at 1600 and 1400 cm^{-1}, which represented C=O, aromatic and C-H stretching, its degradation was promoted as temperature increased. The weak peaks near 1730 and 1030 cm^{-1} were observed for 1:6 mass ratio, these peaks were representative of C–O, C=C, C–C–O stretching, indicating an incomplete degradation and thus needed higher temperatures than the used in this work, but these were removed at lower temperature and mass ratio. Most of the characteristic peaks of biomass lost their intensity because reaction temperature enhanced the formation of intermediate compounds whose were subsequently part of the syngas, as observed at 773.15 K. Regarding B:W mass ratio, some peaks appeared at the lowest mass ratio since the probable poor intimate interaction between water and biomass or intermediate chemicals in comparison with a frequent contact between water and other molecules for high diluted feed. Therefore, those components in the absence of water contact tended to precipitate or promote other reactions, such as polymerization. The absence or low intensity of peaks at high-diluted samples and 773.15 K indicated an adequate biomass dissolution and hydrolysis, together with polymerization of intermediate chemicals.

4. Discussion

Supercritical water gasification of guava biomass was studied in the range of 673.15 to 773.15 K in a batch reactor. Based on the biomass characterization, ash, and moisture

content, it would obtain promising results if temperatures were higher than 673.15 K under supercritical water conditions. Besides, the highest degradation would be expected for lignocellulosic material at higher temperatures based in the weight loss observed in TGA analyses.

Gas production was clearly affected by temperature and B:W mass ratio. The highest gasification efficiency (CGE = 36%, HGE = 58%) and hydrogen gas yield (7.7 mol per 1 kg of guava biomass) were reached at 773.15 K and 1:6 B:W mass ratio. Overall findings are promising results to explore higher temperatures aiming high value-added compounds production for energy purposes. Hydrocarbon production was slightly improved at high temperatures since the dominant effect of the other reactions. The highest values corresponded to methane, followed by ethane, propane, and butane. It would be probable that ethylene and propylene could be in gas phase but in trace amounts, compared with the obtained for ethane and propane. On the opposite, chemicals were produced in detriment of carbon dioxide, whose formation diminished as temperature and mass ratio were rising; besides, low carbon monoxide production was observed along all the reactions. The optimal conditions, high temperature, and high mass ratio favored syngas production, and it could be confirmed throughout LHV. Low concentration and high temperature on feed tend to suppress phenolic compounds formation on solid products, based on the high-diluted biomass waste.

Author Contributions: Conceptualization, A.Z.-M. and O.E.-S.; methodology, S.G.-A. and R.G.-M.; software, R.G.-M. and F.J.V.-S.; validation, S.G.-A. and R.G.-M.; formal analysis, S.G.-A., R.G.-M., S.O.F.-V., and F.J.V.-S.; investigation, S.G.-A., A.Z.-M., and O.E.-S.; resources, A.Z.-M. and O.E.-S.; data curation, R.G.-M. and S.O.F.-V.; writing—original draft preparation, S.G.-A., A.Z.-M., and O.E.-S.; writing—review and editing, O.E.-S.; visualization, O.E.-S.; supervision, A.Z.-M. and O.E.-S.; project administration, O.E.-S.; funding acquisition, A.Z.-M. and O.E.-S. All authors have read and agreed to the published version of the manuscript.

Funding: This research was funded by Instituto Politécnico Nacional. S.G.-A. thanks to Consejo Nacional De Ciencia Y Tecnología for a doctoral scholarship awarded.

Data Availability Statement: Data available on request due to restrictions. The data presented in this study are available on request from the corresponding author. The data are not publicly available due to results are part of thesis project of S.G.-A.

Acknowledgments: Authors thank to Instituto Politécnico Nacional.

Conflicts of Interest: The authors declare no conflict of interest.

References

1. Marcus, Y. *Supercritical Water: A Green Solvent: Properties and Uses*; John Wiley & Sons, Inc.: Hoboken, NJ, USA, 2012. [CrossRef]
2. Desperdicio de Alimentos en México. Available online: http://www.sedesol.gob.mx/boletinesSinHambre/Informativo_02/infografia.html (accessed on 9 April 2021).
3. Guo, Y.; Wang, S.Z.; Xu, D.H.; Gong, Y.M.; Ma, H.H.; Tang, X.Y. Review of catalytic supercritical water gasification for hydrogen production from biomass. *Renew. Sust. Energ. Rev.* **2010**, *14*, 334–343. [CrossRef]
4. Rodriguez Correa, C.; Kruse, A. Supercritical water gasification of biomass for hydrogen production—Review. *J. Supercrit. Fluids* **2018**, *133*, 573–590. [CrossRef]
5. Reddy, S.N.; Nanda, S.; Dalai, A.K.; Kozinski, J.A. Supercritical water gasification of biomass for hydrogen production. *Int. J. Hydrogen Energy* **2014**, *39*, 6912–6926. [CrossRef]
6. Casademont, P.; García-Jarana, M.B.; Sánchez-Oneto, J.; Portela, J.R.; Martínez de la Ossa, E.J. Supercritical water gasification: A patents review. *Rev. Chem. Eng.* **2017**, *33*, 237–261. [CrossRef]
7. Vargas-Mira, A.; Zuluaga-García, C.; González-Delgado, A.D. A technical and environmental evaluation of six routes for industrial hydrogen production from empty palm fruit bunches. *ACS Omega* **2019**, *4*, 15457–15470. [CrossRef]
8. Loppinet-Serani, A.; Reverte, C.; Cansell, F.; Aymonier, C. Supercritical water biomass gasification process as a successful solution to valorize wine distillery wastewaters. *ACS Sustain. Chem. Eng.* **2013**, *1*, 110–117. [CrossRef]
9. Ruya, P.M.; Lim, S.S.; Purwadi, R.; Zunita, M. Sustainable hydrogen production from oil palm derived wastes through autothermal operation of supercritical water gasification system. *Energy* **2020**, *208*, 118280. [CrossRef]

10. Shenbagaraj, S.; Sharma, P.K.; Sharma, A.K.; Raghav, G.; Kota, K.B.; Ashokkumar, V. Gasification of food waste in supercritical water: An innovative synthesis gas composition prediction model based on Artificial Neural Networks. *Int. J. Hydrogen Energy* **2021**, *46*, 12739–12757. [CrossRef]
11. Okolie, J.A.; Nanda, S.; Dalai, A.K.; Berruti, F.; Kozinski, J.A. A review on subcritical and supercritical water gasification of biogenic, polymeric and petroleum wastes to hydrogen-rich synthesis gas. *Renew. Sustain. Energy Rev.* **2020**, *119*, 109546. [CrossRef]
12. Pinkard, B.R.; Gorman, D.J.; Tiwari, K.; Rasmussen, E.G.; Kramlich, J.C.; Reinhall, P.G.; Novosselov, I.V. Supercritical water gasification: Practical design strategies and operational challenges for lab-scale, continuous flow reactors. *Heliyon* **2019**, *5*, e01269. [CrossRef] [PubMed]
13. Wang, S.; Luo, K.; Fan, J. CFD-DEM coupled with thermochemical sub-models for biomass gasification: Validation and sensitivity analysis. *Chem. Eng. Sci.* **2020**, *217*, 115550. [CrossRef]
14. Zhao, L.; Lu, Y. Hydrogen production by biomass gasification in a supercritical water fluidized bed reactor: A CFD-DEM study. *J. Supercrit. Fluids* **2018**, *131*, 26–36. [CrossRef]
15. Tushar, M.S.H.K.; Dutta, A.; Xu, C. Simulation and kinetic modeling of supercritical water gasification of biomass. *Int. J. Hydrogen Energy* **2015**, *40*, 4481–4493. [CrossRef]
16. Xu, C.; Donald, J. Upgrading peat to gas and liquid fuels in supercritical water with catalysts. *Fuel* **2012**, *102*, 16–25. [CrossRef]
17. Okolie, J.A.; Rana, R.; Nanda, S.; Dalai, A.K.; Kozinski, J.A. Supercritical water gasification of biomass: A state-of-the-art review of process parameters, reaction mechanisms and catalysis. *Sustain. Energ. Fuels* **2019**, *5*, 578–598. [CrossRef]
18. Safari, F.; Salimi, M.; Tavasoli, A.; Ataei, A. Non-catalytic conversion of wheat straw, walnut shell and almond shell into hydrogen rich gas in supercritical water media. *Chin. J. Chem. Eng.* **2016**, *24*, 1097–1103. [CrossRef]
19. Nanda, S.; Isen, J.; Dalai, A.K.; Kozinski, J.A. Gasification of fruit wastes and agro-food residues in supercritical water. *Energy Convers. Manag.* **2016**, *110*, 296–306. [CrossRef]
20. Elif, D.; Nezihe, A. Hydrogen production by supercritical water gasification of fruit pulp in the presence of Ru/C. *Int. J. Hydrogen Energy* **2016**, *41*, 8073–8083. [CrossRef]
21. Sheikhdavoodi, M.J.; Almassi, M.; Ebrahimi-Nik, M.; Kruse, A.; Bahrami, H. Gasification of sugarcane bagasse in supercritical water; evaluation of alkali catalysts for maximum hydrogen production. *J. Energy Inst.* **2015**, *88*, 450–458. [CrossRef]
22. Castello, D.; Rolli, B.; Kruse, A.; Fiori, L. Supercritical water gasification of biomass in a ceramic reactor: Long-time batch experiments. *Energies* **2017**, *10*, 1734. [CrossRef]
23. Moghaddam, E.M.; Goel, A.; Siedlecki, M.; Michalska, K.; Yakaboylu, O.; de Jong, W. Supercritical water gasification of wet biomass residues from farming and food production practices: Lab-scale experiments and comparison of different modelling approaches. *Sustain. Energ. Fuels* **2021**, *5*, 1521–1537. [CrossRef]
24. Rashidi, M.; Tavasoli, A. Hydrogen rich gas production via supercritical water gasification of sugarcane bagasse using unpromoted and copper promoted Ni/CNT nanocatalysts. *J. Supercrit. Fluids* **2015**, *98*, 111–118. [CrossRef]
25. Yang, C.; Wang, S.; Yang, J.; Xu, D.; Li, Y.; Li, J.; Zhang, Y. Hydrothermal liquefaction and gasification of biomass and model compounds: A review. *Green Chem.* **2020**, *22*, 8210–8232. [CrossRef]
26. Chen, J.; Fan, Y.; Jiaqiang, E.; Cao, W.; Zhang, F.; Gong, J.; Liu, G.; Xu, W. Effects analysis on the gasification kinetic characteristics of food waste in supercritical water. *Fuel* **2019**, *241*, 94–104. [CrossRef]
27. Molino, A.; Larocca, V.; Valerio, V.; Martino, M.; Marino, T.; Rimauro, J.; Casella, P. Biofuels and bio-based production via supercritical water gasification of peach scraps. *Energy Fuels* **2016**, *30*, 10443–10447. [CrossRef]
28. Chen, J.; Fan, Y.; Zhao, X.; Jiaqiang, E.; Xu, W.; Zhang, F.; Liao, G.; Leng, E.; Liu, S. Experimental investigation on gasification characteristic of food waste using supercritical water for combustible gas production: Exploring the way to complete gasification. *Fuel* **2020**, *263*, 116735. [CrossRef]
29. Su, H.; Kanchanatip, E.; Wang, D.; Zheng, R.; Huang, Z.; Chen, Y.; Mubeen, I.; Yan, M. Production of H_2-rich syngas from gasification of unsorted food waste in supercritical water. *Waste Manag.* **2020**, *102*, 520–527. [CrossRef]
30. Yan, M.; Su, H.; Hantoko, D.; Kanchanatip, E.; Hamid, F.B.S.; Zhang, S.; Wang, G.; Xu, Z. Experimental study on the energy conversion of food waste via supercritical water gasification: Improvement of hydrogen production. *Int. J. Hydrogen Energy* **2019**, *44*, 4664–4673. [CrossRef]
31. Silveira-Junior, E.G.; Perez, V.H.; Rodriguez Justo, O.; Ferreira David, G.; Simionatto, E.; Silva de Oliveira, L.C. Valorization of guava (*Psidium guajava* L.) seeds for levoglucosan production by fast pyrolysis. *Cellulose* **2021**, *28*, 71–79. [CrossRef]
32. ASABE Standards, S319.4. *Method of Determining and Expressing Fineness of Feed Materials by Sieving*; ASABE: St. Joseph, MI, USA, 2008.
33. Claye, S.S.; Idouraine, A.; Weber, C.W. Extraction and fractionation of insoluble fiber from five fiber sources. *Food Chem.* **1996**, *57*, 305–310. [CrossRef]
34. Rani, A.; Kawatra, A. Fiber constituents of some foods. *Plant Foods Hum. Nutr.* **1994**, *45*, 343–347. [CrossRef]
35. Osorio, C.; Forero, D.P.; Carriazo, J.G. Characterisation and performance assessment of guava (*Psidium guajava* L.) microencapsulates obtained by spray-drying. *Food Res. Int.* **2011**, *44*, 1174–1181. [CrossRef]
36. Long, Y.; Ruan, L.; Lv, X.; Lv, Y.; Su, J.; Wen, Y. TG–FTIR analysis of pyrolusite reduction by major biomass components. *Chin. J. Chem. Eng.* **2015**, *23*, 1691–1697. [CrossRef]

37. Kumar, M.; Shukla, S.K.; Upadhyay, S.N.; Mishra, P.K. Analysis of thermal degradation of banana (*Musa balbisiana*) trunk biomass waste using iso-conversional models. *Bioresour. Technol.* **2020**, *310*, 123393. [CrossRef]
38. Ridout, A.J.; Carrier, M.; Görgens, J. Fast pyrolysis of low and high ash paper waste sludge: Influence of reactor temperature and pellet size. *J. Anal. Appl. Pyrolysis* **2015**, *111*, 64–75. [CrossRef]
39. Yang, H.; Yan, R.; Chen, H.; Lee, D.H.; Zheng, C. Characteristics of hemicellulose, cellulose and lignin pyrolysis. *Fuel* **2007**, *86*, 1781–1788. [CrossRef]
40. El Moustaqim, M.; El Kaihal, A.; El Marouani, M.; Men-La Yakhaf, S.; Taibi, M.; Sebbahi, S.; El Hajjaji, S.; Kifani-Sahban, F. Thermal and thermomechanical analyses of lignin. *Sustain. Chem. Pharm.* **2018**, *9*, 63–68. [CrossRef]
41. Yeo, J.Y.; Chin, B.L.F.; Tan, J.K.; Loh, Y.S. Comparative studies on the pyrolysis of cellulose, hemicellulose, and lignin based on combined kinetics. *J. Energy Inst.* **2019**, *92*, 27–37. [CrossRef]
42. Shen, D.K.; Gu, S.; Bridgwater, A.V. Study on the pyrolytic behaviour of xylan-based hemicellulose using TG–FTIR and Py–GC–FTIR. *J. Anal. Appl. Pyrolysis* **2010**, *87*, 199–206. [CrossRef]
43. Chen, W.H.; Eng, C.F.; Lin, Y.Y.; Bach, Q.V. Independent parallel pyrolysis kinetics of cellulose, hemicelluloses and lignin at various heating rates analyzed by evolutionary computation. *Energy Convers. Manag.* **2020**, *221*, 113165. [CrossRef]
44. Chen, Y.; Fang, Y.; Yang, H.; Xin, S.; Zhang, X.; Wang, X.; Chen, H. Effect of volatiles interaction during pyrolysis of cellulose, hemicellulose, and lignin at different temperatures. *Fuel* **2019**, *248*, 1–7. [CrossRef]
45. Chen, W.H.; Wang, C.W.; Ong, H.C.; Show, P.L.; Hsieh, T.H. Torrefaction, pyrolysis and two-stage thermodegradation of hemicellulose, cellulose and lignin. *Fuel* **2019**, *258*, 116168. [CrossRef]
46. Athmaselvi, K.A.; Kumar, C.; Balasubramanian, M.; Roy, I. Thermal, structural, and physical properties of freeze dried tropical fruit powder. *J. Food Process.* **2014**, *2014*, 524705. [CrossRef]
47. Abidi, N.; Cabrales, L.; Haigler, C.H. Changes in the cell wall and cellulose content of developing cotton fibers investigated by FTIR spectroscopy. *Carbohydr. Polym.* **2014**, *100*, 9–16. [CrossRef]
48. Canteri, M.H.; Renard, C.M.G.C.; Le Bourvellec, C.; Bureau, S. ATR-FTIR spectroscopy to determine cell wall composition: Application on a large diversity of fruits and vegetables. *Carbohydr. Polym.* **2019**, *212*, 186–196. [CrossRef]
49. Samy, A.M.; Gopalrao, M. Physiochemical characterization of mucilage obtained from the fresh fruits of *Psidium guajava* L. *Int. J. Phytopharm.* **2015**, *5*, 30–36. [CrossRef]
50. Fitri, R.A.; Wirakusuma, A.; Fahrina, A.; Roil Bilad, M.; Arahman, N. Adsorption performance of low-cost java plum leaves and guava fruits as natural adsorbents for removal of free fatty acids from coconut oil. *Int. J. Eng.* **2019**, *32*, 1372–1378. [CrossRef]
51. Bilba, K.; Ouensanga, A. Fourier transform infrared spectroscopic study of thermal degradation of sugar cane bagasse. *J. Anal. Appl. Pyrolysis* **1996**, *38*, 61–73. [CrossRef]
52. Lazzari, E.; Schena, T.; Marcelo, M.C.A.; Primaz, C.T.; Silva, A.N.; Ferrão, M.F.; Bjerk, T.; Caramão, E.B. Classification of biomass through their pyrolytic bio-oil composition using FTIR and PCA analysis. *Ind. Crops. Prod.* **2018**, *111*, 856–864. [CrossRef]
53. Bilba, K.; Arsene, M.A.; Ouensanga, A. Study of banana and coconut fibers: Botanical composition, thermal degradation and textural observations. *Bioresour. Technol.* **2007**, *98*, 58–68. [CrossRef]
54. Tejado, A.; Peña, C.; Labidi, J.; Echeverria, J.M.; Mondragon, I. Physico-chemical characterization of lignins from different sources for use in phenol–formaldehyde resin synthesis. *Bioresour. Technol.* **2007**, *98*, 1655–1663. [CrossRef]
55. Xu, F.; Yu, J.; Tesso, T.; Dowell, F.; Wang, D. Qualitative and quantitative analysis of lignocellulosic biomass using infrared techniques: A mini-review. *Appl. Energy* **2013**, *104*, 801–809. [CrossRef]
56. Fahey, L.M.; Nieuwoudt, M.K.; Harris, P.J. Predicting the cell-wall compositions of *Pinus radiata* (radiata pine) wood using ATR and transmission FTIR spectroscopies. *Cellulose* **2017**, *24*, 5275–5293. [CrossRef]
57. Tian, Z.; Zong, L.; Niu, R.; Wang, X.; Li, Y.; Ai, S. Recovery and characterization of lignin from alkaline straw pulping black liquor: As feedstock for bio-oil research. *J. Appl. Polym. Sci.* **2015**, *132*, 42057. [CrossRef]
58. Armynah, B.; Tahir, D.; Tandilayuk, M.; Djafar, Z.; Piarah, W.H. Potentials of biochars derived from bamboo leaf biomass as energy sources: Effect of temperature and time of heating. *Int. J. Biomater.* **2019**, *2019*, 3526145. [CrossRef] [PubMed]
59. Kondo, T.; Sawatari, C. A Fourier transform infra-red spectroscopic analysis of the character of hydrogen bonds in amorphous cellulose. *Polymer* **1996**, *37*, 393–399. [CrossRef]
60. Colom, X.; Carrillo, F. Crystallinity changes in lyocell and viscose-type fibres by caustic treatment. *Eur. Polym. J.* **2002**, *38*, 2225–2230. [CrossRef]
61. Toribio Cuaya, H.; Pedraza Segura, L.; Macías Bravo, S.; Gonzalez García, I.; Vasquez Medrano, R.; Favela Torres, E. Characterization of lignocellulosic biomass using five simple steps. *J. Chem. Biol. Phys. Sci.* **2014**, *4*, 28–47, E-ISSN: 2249–1929.
62. Szymanska-Chargot, M.; Zdunek, A. Use of FT-IR spectra and PCA to the bulk characterization of cell wall residues of fruits and vegetables along a fraction process. *Food Biophys.* **2013**, *8*, 29–42. [CrossRef]
63. Traoré, M.; Kaal, J.; Martínez Cortizas, A. Differentiation between pine woods according to species and growing location using FTIR-ATR. *Wood Sci. Tech.* **2018**, *52*, 487–504. [CrossRef]
64. Moosavinejad, S.M.; Madhoushi, M.; Vakili, M.; Rasouli, D. Evaluation of degradation in chemical compounds of wood in historical buildings using FT-IR and FT-Raman vibrational spectroscopy. *Maderas, Cienc. Tecnol.* **2019**, *21*, 381–392. [CrossRef]
65. Horikawa, Y.; Hirano, S.; Mihashi, A.; Kobayashi, Y.; Zhai, S.; Sugiyama, J. Prediction of lignin contents from infrared spectroscopy: Chemical digestion and lignin/biomass ratios of *Cryptomeria japonica*. *Appl. Biochem. Biotechnol.* **2019**, *188*, 1066–1076. [CrossRef]

66. Kizil, R.; Irudayaraj, J.; Seetharaman, K. Characterization of irradiated starches by using FT-Raman and FTIR spectroscopy. *J. Agric. Food Chem.* **2002**, *50*, 3912–3918. [CrossRef]
67. Sun, R.C.; Fang, J.M.; Tomkinson, J.; Jones, G.L. Acetylation of wheat straw hemicelluloses in *N*,*N*-dimethylacetamide/LiCl solvent system. *Ind. Crops. Prod.* **1999**, *10*, 209–218. [CrossRef]
68. Faix, O. Classification of lignins from different botanical origins by FT-IR spectroscopy. *Holzforschung* **1991**, *45*, 21–27. [CrossRef]
69. Zhao, Y.; Feng, D.; Zhang, Y.; Huang, Y.; Sun, S. Effect of pyrolysis temperature on char structure and chemical speciation of alkali and alkaline earth metallic species in biochar. *Fuel Process. Technol.* **2016**, *141*, 54–60. [CrossRef]